Lecture Note II (1992)
Graduate School of Science
Kyoto University

Nonlinear Waves in Flagella

Masatoshi Murase

Yukawa Institute for Theoretical Physics
Kyoto University

A flagellum suspended in a viscous fluid is considered to be a class of nonlinear distributed systems. Within a local system shear motion occurs back and forth, which results from an alternate turning "on" and "off" of opposed-active elements. Each active element is characterized by *excitability* in that shear motion is triggered only by a *superthreshold* shear displacement. Once shear motion is initiated at one end of the system, it is successively triggered to the other end. These triggering events cause the propagation of bending waves. The dynamics of such propagating waves are described by the forth-order partial differential equation. From a point of view of nonlinear dynamics, it is useful to consider this equation to be a possible extension of the *Kuramoto-Sivashinsky* equation which describes *self-turbulization* phenomena in different physical contexts. Numerical simulations for the present flagellar model reveal (i) the reversal of the direction of propagating waves and (ii) the *soliton-like* non-annihilating waves. These simulation results are qualitatively in good agreement with experimental observations.

1. Introduction

Flagella not only show regular wave phenomena like base-to-tip bending wave propagation, but also exhibit irregular wave phenomena such as the reversal of propagating waves [1-5] and non-annihilating waves [2,6]. However, most of the theoretical work has been focused only on the regular wave phenomena rather than potentially important irregularity in the flagellar dynamics [7-14]. Recently, we have developed a flagellar model which contains a series of opposed-excitable units [15]. The model appeared to be hard to control regular wave patterns. This occurs because there are two different types of interactions among local systems: one is *attractive* and the other is

repulsive. The competition between the two interactions causes the spatio-temporal irregularity. Similar situation appears in the Kuramoto-Sivashinsky equation which describes self-turbulization phenomena in different physical contexts [16-25]. In fact, the present model equation can be reduced to the Kuramoto-Sivashinsky equation under a certain extent. In the present paper, irregular nature inherent in this model system has been investigated. Numerical simulations for this model show that (i) the direction of propagating waves is successively reversed and (ii) the two waves propagating in the opposite directions pass through on collision like solitons. The present studies would provide us with a bridge between cell biology and nonlinear science.

2. Model system

Since the model for a flagellum has been developed elsewhere [15,26,27], the final form of equations are given as follows:

$$\frac{\partial^2(S - \gamma\dot{\sigma})}{\partial s^2} + E_B\frac{\partial^4\sigma}{\partial s^4} + C_N\frac{\partial\sigma}{\partial t} = 0 \qquad (1a)$$

$$S = F_I n_I + F_{II}(1 - n_I) - K_c(\sigma - \sigma_0) \qquad (1b)$$

$$F_I = Q_I(\sigma - \sigma_1)(\sigma - \sigma_2)(\sigma_c - \sigma) \qquad (1c)$$

$$F_{II} = Q_{II}(\sigma - \sigma'_1)(x - \sigma'_2)(\sigma'_c - \sigma) \qquad (1d)$$

$$n_I = \begin{cases} 1 & 0 < \sigma \le S_1 \\ 0 & S_1 < \sigma < 1 \end{cases} \quad \text{(if initially } n_I = 0 \text{ for } \sigma > S_1) \qquad (1e)$$

$$n_I = \begin{cases} 1 & 0 < \sigma \le S_2 \\ 0 & S_2 < \sigma < 1 \end{cases} . \quad \text{(if initially } n_I = 1 \text{ for } \sigma < S_2) \qquad (1f)$$

Equation (1a) describes the dynamics of a flagellum suspended in a viscous fluid, where S is the shear force, σ the shear (as a function of arc length s and time t), E_B the bending resistance, C_N the external viscous drag coefficient and γ is the internal viscous drag coefficient. The shear force, S, is represented by equation (1b) which consists of the active shear force in subsystem I (i.e. the first term of the right-hand side), the active shear force in opposed subsystem II (i.e. the second term) and the passive restoring force (i.e. the third term).

The cubic force-shear relationships for subsystems I and II are given by equations (1c) and (1d), respectively. Figure 1A illustrates these cubic functions. The form of the cubic function is essential for the excitable nature because for example in subsystem I there is a threshold position at σ_c, below which σ goes to one stable state at σ_1 (resting state) and above which it goes to the other state at σ_2 (active state). The resultant transition from the resting state to the active state corresponds to active shear motion. The same is true for subsystem II except for the shear direction.

Each subsystem is assumed to possess "on" and "off" states. It switches between these two states when the shear passes critical values (called *switching points*). When the shear falls below S_1 subsystem I is turned "on" ($n_I = 1$) and maintains its state until the shear rises above S_2, and is turned "off" ($n_I = 0$). By setting $S_1 \neq S_2$, either "on" or "off" can occur depending on the "history" of the subsystem. This history-dependent characteristic is called *hysteresis*. This hysteresis switching process can be described by the *binary* function of σ, which is described by equations (1e) and (1f). Figure 1B illustrates these binary functions.

In obtaining solutions to equations (1a-f), the free end boundary conditions are used:

$$\left.\frac{\partial^2\sigma}{\partial s^2}\right|_{s=0} = 0 \; ; \; \left.\frac{\partial\sigma}{\partial s}\right|_{s=0} = 0 \qquad (1g)$$

$$\left.\frac{\partial^2\sigma}{\partial s^2}\right|_{s=L} = 0 \; ; \; \left.\frac{\partial\sigma}{\partial s}\right|_{s=L} = 0 \; . \qquad (1h)$$

Here, s is the arc length along the flagellum and L is the length of the flagellum. Boundary conditions (1g) and (1h) represent that all the moments and forces vanish at both ends.

It should be noticed that equation (1a) can be reduced to the so-called reaction-diffusion equation when $\gamma \neq 0$ and $C_N = 0$ [see 28]:

$$\gamma\frac{\partial\sigma}{\partial t} = E_B\frac{\partial^2\sigma}{\partial s^2} + S \qquad (1a')$$

and the boundary conditions (1g) and (1h) become

$$\left.\frac{\partial\sigma}{\partial s}\right|_{s=0} = 0 \qquad (1g')$$

$$\left.\frac{\partial\sigma}{\partial s}\right|_{s=L} = 0 \; . \qquad (1h')$$

Boundary conditions (1g') and (1h') require zero curvature at s = 0 and L.

3. Instability inherent in the model system

Before attempting to demonstrate wave phenomena by solving equations (1a-h), it is useful to examine instability arising from the model system. To understand such an instability two types of

simulations were performed, either with only internal viscosity (i.e. $\gamma \neq 0$ and $C_N = 0$) or only external viscosity (i.e. $\gamma = 0$ and $C_N \neq 0$).

For numerical simulations, a 50-μm model flagellum is divided into 50 segments of length 1 μm. The simulation results did not change when the number of segments of the model flagellum was increased.

In the following simulations the system had only passive elastic links along its entire length (i.e. $Q_I = Q_{II} = 0$), and a completely straight configuration was used as an initial condition. In the first type of simulation, a positive shear force (S = 50 pN) was applied to the middle segment of the flagellum (at s = 25 μm) under free end boundary conditions.

Figure 2 illustrates the relative shear plotted against the arc length, s, immediately (0.01 msec) after a step increase in shear force at s = 25 μm. The simulated shear distribution is spiky because a short time interval is allowed between the onset of the shear force and the time when the resultant shear distribution is calculated. By adopting this simulation technique we can ignore the effects of the elastic bending resistance, and hence neglect the effects of the terms involving E_B in equations (1a) and (1a'). At zero external viscosity but with internal viscosity, a positive shear force can only lead to positive shear displacements (Fig.2A). In the presence of external viscosity only, however, positive shear force can lead to negative shear in nearby regions (Fig.2B). This difference is clearly understood by considering the finite-difference approximation as follows.

Let space, s, and time, t, be made discrete by adopting $s = i\Delta s$ and $t = j\Delta t$, where i and j are integers, and Δs and Δt are the respective steps of the mesh along the s- and t-axis. Now $\sigma_{i,j}$ is used to denote $\sigma(i\Delta s, j\Delta t)$. Similarly, let S_i denote $S(s = i\Delta s)$. For convenience we assume $\Delta s = \Delta t = 1$. The final form of the finite-difference scheme for equation (1a') under a single point force at i-th segment (at s = 25 μm in Fig.2A) is:

$$\sigma_{i,j+1} = \sigma_{i,j} + S_i \qquad (2)$$

and the form of equation (1a) is written as follows:

$$\sigma_{i,j+1} = \sigma_{i,j} + 2S_i \qquad (3a)$$
$$\sigma_{i-1,j+1} = \sigma_{i-1,j} - S_i \qquad (3b)$$
$$\sigma_{i+1,j+1} = \sigma_{i+1,j} - S_i \,. \qquad (3c)$$

Equation (2) predicts that σ_i increases when $S_i > 0$. In contrast equations (3a-c) predict that σ_i increases, but at the same time σ_{i-1} and σ_{i+1} decrease even if $S_i > 0$.

In the second type of simulation, an abrupt change in shear (not shear force) was applied at s = 0 under the clamped end boundary conditions. When there is only internal viscosity the clamped condition at a certain shear σ_0 is described by:

$$\sigma|_{s=0} = \sigma_0 \ . \qquad (4)$$

While when there is only external viscosity the clamped conditions are:

$$\left.\frac{\partial^3\sigma}{\partial s^3}\right|_{s=0} = 0 \ ; \ \sigma|_{s=0} = \sigma_0 \ . \qquad (5)$$

Figure 3 shows shear distribution some time (1 msec) after a step change in shear at s = 0 (σ_0 is changed from 0 to 0.5). Since all the segments are passive, the shear force, S, is almost zero. The terms involving S can be neglected in equations (1a) and (1a'). An abrupt change in shear at s = 0 is transmitted via an elastic coupling. A long period (1 msec) was allowed to proceed in order to obtain the shear distribution affected by the secondary effects of the elastic coupling. If there is only an internal viscosity, then shear is always in the same direction as the abrupt change (dotted curve). If, however, an external viscosity is present (with no internal viscosity), an external shear force develops in a distal region which causes shear in the opposite direction, though shear in the segment closer to the basal end is in the same direction as the abrupt change (solid curve).

This difference is again understood by considering the finite-difference form for each original partial differential equation. The finite-difference form of equation (1a') is:

$$\sigma_{i,j+1} = \sigma_{i,j} + E_B(\sigma_{i-1,j} - 2\sigma_{i,j} + \sigma_{i+1,j}) \qquad (6)$$

and the form of equation (1a) is written as

$$\sigma_{i,j+1} = \sigma_{i,j} - E_B[(\sigma_{i-2,j} - 2\sigma_{i-1,j} + \sigma_{i,j}) - 2(\sigma_{i-1,j} - 2\sigma_{i,j} + \sigma_{i+1,j}) + (\sigma_{i,j} - 2\sigma_{i+1,j} + \sigma_{i+2,j})] \ . \qquad (7)$$

Equations (6) and (7) show the *attractive* interaction between the nearest neighbor segments, because the right-hand side of equation (6) is decomposed into

$$E_B(\sigma_{i-1,j} - 2\sigma_{i,j} + \sigma_{i+1,j}) = -E_B(\sigma_{i,j} - \sigma_{i+1,j}) - E_B(\sigma_{i,j} - \sigma_{i-1,j}) \ . \qquad (8)$$

As a result, positive shear at s = 0 always induces positive shear in regions nearby. On the contrary, the average shear defined by

$$\bar{\sigma}_{i,j} = \sigma_{i-1,j} - 2\sigma_{i,j} + \sigma_{i+1,j} \qquad (9)$$

shows the *repulsive* interactions between the average regions nearby, because the right-hand side of equation (7) is decomposed into

$$- E_B(\bar{\sigma}_{i-1,j} - 2\bar{\sigma}_{i,j} + \bar{\sigma}_{i+1,j}) = E_B(\bar{\sigma}_{i,j} - \bar{\sigma}_{i+1,j}) + E_B(\bar{\sigma}_{i,j} - \bar{\sigma}_{i-1,j}) . \quad (10)$$

Equation (7) suggests that positive shear at s = 0 induces positive shear in the region nearby, yet at the same time negative shear via its average shear. This situation seems to be somewhat analogous to phenomena with *short range activation* and *long range inhibition* in neurophysiology, population dynamics, and morphogenesis [29]. For real simulations, three terms in equation (1a) must be taken into account. One can therefore expect that complex dynamical behavior will appear in the flagellar system described by equation (1a).

4. Propagating waves

4.1 Self-organization of propagating waves with only internal viscosity

To demonstrate self-organization of propagating waves, a self-oscillatory basal end is combined with 49 segments exhibiting excitable behavior in the model described by equation (1a'). This type of model is easily developed by adopting K_e = 60 pN/24 nm at s = 1 μm and K_e = 1 pN/24 nm for 1 < s < 50 μm, because the proximal segment with a large K_e value acts as a *pacemaker* which can periodically stimulate the rest of the flagellum. The simulations were performed starting from a straight-formed flagellum under free end boundary conditions.

For the convenience of the following discussion, we shall introduce the space-time diagram as shown in Figure 4. This figure depicts the positions of waves (where the regions σ > 0.5 are plotted by bars) as a function of time, t, and space, s. There is only a single bar at a given time for 0 < t < 45 msec corresponding to a single bend. As time proceeds, the bar moves to the right which is associated with bend propagation. A steady-state waveform is attained as the first bend reaches the tip. As a result there are two bars (corresponding to two bends) at any time for t > 45 msec. They continuously move to the right. The degree of successive shifts of bars in the space-time diagram indicates the velocity of bend propagation. The regular spatio-temporal patterns suggest that the system reaches a stable cycle of steady-state bend initiation and propagation.

4.2 The reversal of propagating waves with only external viscosity.

It is of interest to know what happens in the absence of the internal viscosity. Under the conditions with the external visocity, the model is started from a straight configuration at t = 0. Figure 5 shows that bend propagation occurs first from base to tip and then the direction is reversed at the first arrow (about t = 300 msec). These tip-to-base propagating waves are further replaced by the base-to-tip propagating waves at the second arrow (about t = 600 msec). This

kind of reversal of bend propagation occurs at 300 - 400 msec intervals as long as the computer simulation persists.

The frequency of this reversal depends on the stiffness of the elastic component at the base. The stiffness of the basal elastic component determines the characteristic frequency of the self-oscillation, so that the basal region affects the duration of the reversal. An alternative way to change the frequency of the reversal of the direction of propagating waves is to insert the "passive" region at the tip end. This kind of passive region amounts to the structural asymmetry of the flagellum. From a functional point of view, the passive region acts as "buffer" which absorbs viscosity-induced perturbations. For example, the model with a passive region 5 μm long shows shorter duration of the reversal than the model without the passive region. As the length of the passive region is increased, the possibility for the reversal of bend propagation decreases markedly. A 10-μm passive region is sufficient to ensure unidirectional bend propagation [15].

Suppose we have a "homogeneous" flagellum without the passive or the self-oscillatory region, but with excitability throughout the length of the flagellum. This model is obtained when the stiffness at the basal segment is reduced from K_e = 60 to 1 pN/24 nm. Of course this "homogeneous" excitable system can not develop bending waves without superthreshold perturbations if the flagellum is initially straight. Once the flagellum was slightly deformed, however, bending waves were developed. Under these conditions the model showed the reversal of propagating waves at about 1200-msec intervals.

These simulations suggest that the flagellar structure is highly responsible for the dynamical behavior. Boundary conditions seem to be of secondary importance. Indeed there was an interesting observation by Brokaw [30], in which removal of the normal distal end of the flagellum interfered with its ability to generate base-to-tip propagating waves. Omoto and Brokaw [31] also observed a clear "end effect", which involves a rapid unbending of bends that have reached the distal end of the flagellum lacking a "terminal" region.

Besides the reversal of the direction of propagating waves, the patterns in Fig.5 are slightly different from those in Fig.4 in the following ways. First, the velocity of bend propagation would fluctuate as the slope of successive bars is not constant. There is some experimental evidence that the bend propagation velocity in the basal and distal region is lower than the velocity in the mid-region of the flagellum. This refers to non-uniform bend propagation [32]. Our results may be relevant to this experimental observation. Second, the wavelength would fluctuate as the width of the bars along the s-axis is not constant. Third, the beat frequency would fluctuate as the "black-white" interval along the t-axis is not constant.

These three characteristics are not obvious as long as we take only a small number of snapshots of flagellar shape at different instants. Furthermore, the flagellar shapes in the (x, y) coordinate are obtained by an integral form:

$$x(s) = \int_0^s \cos(\sigma)\, ds, \quad y(s) = \int_0^s \sin(\sigma)\, ds. \tag{11}$$

so that if there are spatial fluctuations on the sliding patterns they smooth away when they are transformed into the shapes [see 15]. For these reasons the above characteristics have not been discussed deeply.

Although experimental data show irregularity, it has been ascribed to the nature of random noise [32]. However the present study suggests that these fluctuations arise in a deterministic mathematical model. It seems that they are not caused by random noise nor numerical errors, but are inherent in the system under the influence of external viscosity.

5. Interaction of two waves propagating in the opposite directions

It has been observed that two waves traveling in opposite directions along the flagellum under abnormal conditions where the viscosity of the medium is increased [2] or when some chemical agent is added [6]. When two such waves meet they appear to be frozen, but do not annihilate each other. These observations raise a problem concerning the interaction between the two waves. From a theoretical modelling point of view, however, no attempts have been made to solve this problem. It is, therefore, important to know whether or not two waves moving in opposite directions annihilate each other.

Simulations were carried out under two different situations: (i) with only internal viscosity; and (ii) with only external viscosity. The model was allowed to develop two bends propagating in opposite directions by applying stimuli at both ends. If there is only internal viscosity, two oppositely directed bends annihilate each other upon collision (Figure 6). Each bend has a leading edge and a trailing edge. In the leading edge of each bend, subsystem I is turned "on" and subsystem II is turned "off", while in the trailing edge the reverse holds. The waves move in accordance with the operation of these "on-off" switches. This switching operation continuously propagates, so that the system is completely reset after the bend passes through. As a result, the two waves seem to annihilate, leaving the system at rest. This phenomenon is analogous to the annihilation of action potentials in nerve systems [33,34] and chemical waves such as the Belousov-Zhabotinsky reaction [35-39].

If there is external viscosity, instead of internal viscosity, the waves appear to pass through one another (Figure 7). The waves move slowly because only a small region at the trailing edge of each bend contributes to active sliding. The active region is small because viscous forces oppose the force required to reach the switching point. Thus both peak height and width in the σ-s curves become smaller as the waves approach one another, as indicated by less smoothness. As the waves approach sufficiently close, the bends appear to merge, and switching occurs in many segments in the region of the collision.

Since the resting state is not stable enough in these segments, sliding in the opposite direction, caused by subsystem II, occurs. After the collision, the number of segments contributing to active sliding is four times larger than before the collision, so wave speed is about four-fold faster.

Non-annihilating waves appear because the operation of "on-off" switches is not continuously propagated but sometimes skips several segments due to viscosity-induced perturbations. As a result, the system never returns to the resting state, but instead some segments are spontaneously activating. By using the two-component reaction-diffusion model, Tuckwell [40] found solitary wave solutions with soliton-like properties when "on-off" switches were introduced into the model. Because the system 'sees' the new source functions during the collision of two solitary waves due to a number of "on-off" switches, it is possible that solitary waves emerge from the collision.

Tuckwell [40] also found that with slightly asymmetric initial data, when two waves collided, one wave more or less destroyed the other and continued to propagate after the collision. Similar phenomena appeared in the present model behavior when the direction of bend propagation was reversed. As already shown in Fig.5, the flagellar system happened to initiate the tip-to-base propagating wave. This destroyed the base-to-tip propagating wave since two waves are slightly different in the shape.

6. Discussion

To understand the dynamical aspects of external viscosity-induced perturbations, the model is started from the same initial conditions with only internal viscosity (Fig.8A) or only external viscosity (Fig.8B). If there is only internal viscosity, the flagellum becomes quiescent when the bend reaches the tip. On the contrary, if there is only external viscosity, viscosity-induced perturbations strongly influence the basal end to move up and down. Since this rhythmic motion continues for ever, the flagellum never returns to the resting state.

It is now clear that the ratio between γ and C_N in equation (1a) plays an important role in determining the dynamical behavior of the model. If $\gamma >> C_N$ the term $-\gamma\dot{\sigma}$ stabilizes the solution, and hence the dynamical behavior is similar to that obtained by equation (1a'). If $\gamma << C_N$ the behavior is analogous to that generated by equation (1a) with $\gamma = 0$ and $C_N \neq 0$.

The forth-order partial differential equations of this kind appear in various ways. The general form of these equations is:

$$\frac{\partial \phi}{\partial t} = A\frac{\partial^2 \phi}{\partial s^2} - B\frac{\partial^4 \phi}{\partial s^4} + F(\phi) \qquad (12)$$

where ϕ is a state variable defined at space, s, and time, t, A and B are constants, and $F(\phi)$ is some nonlinear function. This type of equation is sometimes called the *generalized reaction diffusion* equation [29], but also named the *Kuramoto-Sivashinsky* equation [16-20]. Similar equations are also proposed in quite different contexts [21-25]. The second order term in equation (12) corresponds to the diffusion process. When $A > 0$ spatial perturbations are stabilized (*normal diffusion*), though when $A < 0$ they are destabilized (*negative diffusion*).

It is instructive to consider that the internal shear force, S, is proportional to the shear, σ, as a linearized form of the cubic force-distance function in equation (1b-d). Then, equation (1a) is analogous to equation (12) when $\gamma = 0$. This situation corresponds to negative diffusion, leading to instability. Indeed, Brokaw [8] pointed out that the presence of internal viscosity (i.e. $\gamma > 0$) can stabilize the wavelength. The stable wavelength arises because the situation $\gamma > 0$ amounts to the normal diffusion, and hence stabilization.

To demonstrate regular base-to-tip wave propagatin, most of the theoretical models have assumed that the shear force, S, is controlled by the curvature of the flagellum [7-13]. Now consider the effects of the *curvature control* on solutions to equation (1a). There are only even powers of the space derivatives, so that symmetry holds with respect to space, s. (Both the equation and boundary conditions are invariant under the spatial inversion $s \rightarrow - s$.) As a result, base-to-tip and tip-to-base waves are potentially equivalent. One way by which unidirectional propagated waves are obtained is to introduce the curvature feedback control. The curvature of the flagellum can only be defined when two separate positions are specified (or mathematically, the curvature, κ, is defined as a space derivative of shear: $\kappa = \partial\sigma/\partial s$). This automatically induces the spatial coordination in violation of the $s \rightarrow - s$ symmetry because of the first space derivative, $\partial\sigma/\partial s$, which is necessary in maintaining bend propagation in one direction. An alternative way in demonstrating unidirectional bend propagation is to take into account the structural asymmetry such as the basal elastic component and the passive terminal piece.

As a concrete example, let us consider an flagellum with self-oscillatory behavior. By adopting K_e = 60 pN/24 nm and the cubic force-distance function for $0 < s < 50$ μm, we can obtain a model with "homogeneously" distributed self-oscillatory segments. Simulations were carried out from straight-line initial conditions in the following three cases. When the flagellum is "homogeneous" two waves initiate at both ends and propagate in opposite directions (Fig.9A). If the distal 10-μm of the flagellum was replaced by the passive region without active force-generating systems, then unidirectional bend propagation can occur (Fig.9B). If the curvature control mechanisms are introduced such that subsystem I is turned "off" when $\kappa > 0$ and

turned "on" when $\kappa < 0$, unidirectional bend propagation can also occur (Fig.9C).

By incorporating the curvature feedback control into theoretical models, unidirectional bend propagation has been demonstrated. Although these models successfully generate bend propagation from base to tip, important and interesting aspects have been missed. In the absence of the curvature control mechanism, models lose their ability to propagate bending waves in one direction. The failure of unidirectional bend propagation is not a 'defect' of the models, but a 'merit' inherent in the system suspended in the viscous medium. There is the possibility that such a system shows a wide variety of spatio-temporal behaviors. The complex dynamical behavior of this kind is one of the most interesting topics in modern physics, biology and chemistry.

References

[1] G. J. Douglas and M. E. J. Holwill, J. Mechanochem. Cell Motility, 1 (1972) 213.
[2] M. E. J. Holwill, J. Exp. Biol. 42 (1965) 125.
[3] M. E. J. Holwill and J. L. McGregor, J. Exp. Biol. 60 (1974) 437.
[4] M. E. J. Holwill and J. L. McGregor, Nature 255 (1975) 157.
[5] M. E. J. Holwill and J. L. McGregor, J. Exp. Biol. 65 (1976) 229.
[6] J. Alexander and R. G. Burns, Nature 305 (1983) 313.
[7] C. J. Brokaw, J. Exp. Biol. 55 (1971) 289.
[8] C. J. Brokaw, Proc. Nat. Acad. Sci. U.S.A. 72 (1975) 3102.
[9] C. J. Brokaw, Biophys. J. 16 (1976) 1029.
[10] C. J. Brokaw, Symp. Soc. Exp. Biol. 35 (1982) 313.
[11] C. J. Brokaw, Biophys. J. 48 (1985) 633.
[12] M. Hines and J. J. Blum, Biophys. J. 23 (1978) 41.
[13] M. Hines and J. J. Blum, Biophys. J. 25 (1979) 421.
[14] R. Rikmenspoel, J. Theor. Biol. 96 (1982) 617.
[15] M. Murase, M. Hines and J. J. Blum, J. Theor. Biol. 139 (1989) 413.
[16] Y. Kuramoto, Chemical Oscillations, Waves, and Turbulence (Springer-Verlag, Berlin, 1984).
[17] D. M. Michelson and G. I. Sivashinsky, Acta Astronautica 4 (1977) 1207.
[18] G. I. Sivashinsky, Acta Astronautica 4 (1977) 1177.
[19] G. I. Sivashinsky, SIAM J. Appl. Math. 39 (1980) 67.
[20] G. I. Sivashinsky, Phisica D 17 (1985) 243.
[21] A. Pumir, P. Manneville and Y. Pomeau, J. Fluid Mech. 135 (1983) 27.
[22] H.-C. Chang, Chem. Engng. Sci. 41 (1986) 2463.
[23] L.-H. Chen and H.-C. Chang, Chm. Engng. Sci. 41 (1986) 2477.
[24] A. P. Hooper and R. Grimshaw, Phys. Fluids 28 (1985) 37.
[25] J. M. Hyman and B. Nicolaenko, Physica D 18 (1986) 113.
[26] M. Murase, J. Theor. Biol. 146 (1990) 209.
[27] M. Murase, Dynamics of Cellular Motility (Manchester University Press, Oxford, inpress).
[28] M. Murase and H. Shimizu, J. Theor. Biol. 119 (1986) 409.
[29] J. D. Murray, Mathematical Biology (Springer-Verlag, Berlin, 1989).
[30] C. J. Brokaw, J. Exp. Biol. 43 (1965) 155.

[31] C. K. Omoto and C. J. Brokaw, J. Cell Sci. 58 (1982) 385.
[32] C. J. Brokaw, J. Exp. Biol. 53 (1970) 445.
[33] I. Tasaki, Proc. R. Soc. Lond. A209 (1951) 447.
[34] G. Matsumoto, K. Aihara and T. Utsunomiya, J. Phys. Soc. Jpn, 51 (1982) 942.
[35] Y. Kuramoto and T. Yamada, Prog. Theor. Phys. 56 (1976) 724.
[36] A. T. Winfree, The Geometry of Biological Time (Springer-Verlag, Berlin, 1980).
[37] A. T. Winfree, When Time Breaks Down. The Three-Dimensional Dynamics of Electrochemical Waves and Cardiac Arrhythmias (Princeton University Press, Princeton, 1987).
[38] V. S. Zykov, Simulation of Wave Processes in Excitable Media (Manchester University Press, Oxford, 1987).
[39] L. Glass and M. C. Mackey, From Clocks to Chaos: The Rhythms of Life (Princeton University Press, Princeton, 1988).
[40] H. C. Tuckwell, SIAM J. Appl. Math. 39 (1980) 310.

Figure Captions

Figure 1

The cubic force-shear and hysteresis switching functions. (A): The active force is shown as a function of the (dimensionless) shear, σ. The solid line shows the force, F_I, for sliding in the forward direction (increasing σ), and the dotted line the force, F_{II}, for sliding in the backward direction (decreasing σ). The force-shear functions are: $F_I = Q_I(\sigma - 0.1)(\sigma - 1)(0.3 - \sigma)$, and $F_{II} = Q_{II}(\sigma - 0.9)(\sigma)(0.7 - \sigma)$ with $Q_I = Q_{II} = 250$ pN. (B): The hysteresis switch as a function of σ. The binary function is defined in the region $S_1 < \sigma < S_2$, where $S_1 = 0.2$ and $S_2 = 0.8$. The value depends on what direction the region is entered. Note that $n_I + n_{II} = 1$ for each direction of movement.

Figure 2

Relative shear, $\sigma(s)/\sigma(25)$, as a function of space, s, after an application of a point force of 50 pN at s = 25 μm under free end boundary conditions. An initially straight flagellum has only passive elastic links, i.e., K_e = 1 pN/24 nm, $Q_I = Q_{II} = 0$ and E_B = 400 pNμm^2. A single point force of 50 pN is applied to the middle segment at s = 25 μm. The relative shear is plotted 0.01 msec after the stimulus. (A): There is only internal viscosity, i.e., γ = 50 pN msec/24 nm and $C_N = 0$. Positive shear force always causes positive shear. (B): There is only external viscosity, i.e., $\gamma = 0$ and C_N = 5 pNmsec/μm^2. Positive shear force induces negative shear in the nearby region.

Figure 3

Shear, σ, as a function of s after an abrupt change of shear at the basal end, such that $\sigma_0 = 0.5$ under the clamped end boundary conditions. An initially straight flagellum with only passive elastic links K_e = 1 pN/24 nm and E_B = 400 pNμm^2 is subjected to an abrupt change in the shear at the base. The distribution of shear 1 msec after the proximal end is displaced. Note that $\sigma_0 = 0$ at t = 0 for 0 < s < 50 μm. The dotted line shows $\sigma(s)$ with only internal viscosity, i.e., γ = 50 pN msec/24 nm and $C_N = 0$. The solid line shows $\sigma(s)$ with only external viscosity, i.e., $\gamma = 0$ and C_N = 5 pNmsec/μm^2.

Figure 4

Positions of waves as a function of time, t (in msec), and space, s (in μm). The initially straight flagellum was allowed to develop its bending waves. The parameters are: E_B = 300 pNμm^2, γ = 100

pNmsec/24 nm, $Q_I = Q_{II} = 300$ pN, $\sigma_1 = 0.15$, $\sigma_2 = 1$, $\sigma_c = 0.25$, $\sigma'_1 = 0.85$, $\sigma'_2 = 0$, and $\sigma'_c = 0.75$. The properties of the flagellum vary along its length as follows: $K_e = 60$ pN/24 nm for $s = 1$ μm and $K_e = 1$ pN/24 nm for $1 < s < 50$ μm. This is equivalent to an oscillatory region in the first segment, an excitable region in segments 2 - 50. The regions $\sigma > 0.5$ are plotted by bars. As time proceeds, the groups of bars move toward the right reflecting the fact that bending waves initiated at the base (at the left end) propagate toward the tip (the right end). The schematic representation of this flagellum is shown in the bottom panel.

Figure 5

Reversal of the direction of propagating waves under free end boundary conditions in the presence of the external viscosity. The parameters are: $E_B = 400$ pNμm^2, $C_N = 5$ pNmsec/μm^2, $Q_I = Q_{II} = 270$ pN and $K_e = 1$ pN/24 nm. Positions of waves are depicted as a function of time, t (in msec), and space, s (in μm). The regions $\sigma > 0.5$ are plotted by bars. As time proceeds, first base-to-tip bend propagation occurs and then tip-to-base bend propagation appears at about t = 300 msec. At about t = 600 msec base-to-tip bend propagation occurs. The schematic representation of this flagellum is shown in the bottom panel.

Figure 6

Annihilation of two waves propagating in opposite directions at zero external viscosity under free end boundary conditions. The parameters are: $Q_I = Q_{II} = 290$ pN, $E_B = 300$ pNμm^2, $L = 100$ μm, $C_N = 0$, $\gamma = 100$ pN msec/24 nm, and $K_e = 1$ pN/24 nm. σ is plotted as a function of space, s, at 1-msec intervals. Time proceeds from front to back.

Figure 7

Soliton-like behavior at non-zero external viscosity under free end boundary conditions. The parameters are: $Q_I = Q_{II} = 400$ pN, $E_B = 400$ pNμm^2, $L = 100$ μm, $C_N = 5$ pNmsec/μm^2, $\gamma = 0$, and $K_e = 1$ pN/24 nm. σ is plotted as a function of space, s, at 2-msec intervals. Time proceeds from front to back.

Figure 8

Dynamical behavior of a "homogeneous" excitable flagellum under free end boundary conditions. σ is plotted as a function of space, s, at 5-msec intervals. The flagellum has only excitable segments, i.e., $K_e = 1$ pN/24 nm, $Q_I = Q_{II} = 250$ pN and $E_B = 400$ pNμm^2 for $0 < s < 50$ μm. The model is started from the same initial conditions. (A): There

is only internal viscosity, i.e., γ = 100 pN msec/24 nm and C_N = 0. The flagellum becomes "quiescent" when the bend propagates to the tip. (B): There is only external viscosity, i.e., γ = 0 and C_N = 5 pNmsec/μm^2. Due to external viscosity-induced perturbations the basal end beats up and down, which leads to continuous bend initiation.

Figure 9

Dynamical behavior of the self-oscillatory flagellum under free end boundary conditions. σ is plotted as a function of space, s, at 20-msec intervals. The flagellum has only self-oscillatory segments, i.e., K_e = 60 pN/24 nm, $\mathcal{Q}_I = \mathcal{Q}_{II}$ = 250 pN and E_B = 400 pNμm^2 for 0 < s < 50 μm. The model is started from the same straight configuration. (A): The "homogeneous" self-oscillatory flagellum is allowed to develop bending waves. (B): The self-oscillatory flagellum with a 10-μm long passive region at the tip. Unidirectional bend propagation results from this asymmetric structure. (C): The "homogeneous" self-oscillatory flagellum under the influence of the curvature control mechanism, in which $\mathcal{Q}_I = 0$ for $\kappa > 0$ and $\mathcal{Q}_{II} = 0$ for $\kappa < 0$. Unidirectional bend propagation is caused by the feedback function which is asymmetric about $\kappa = 0$.

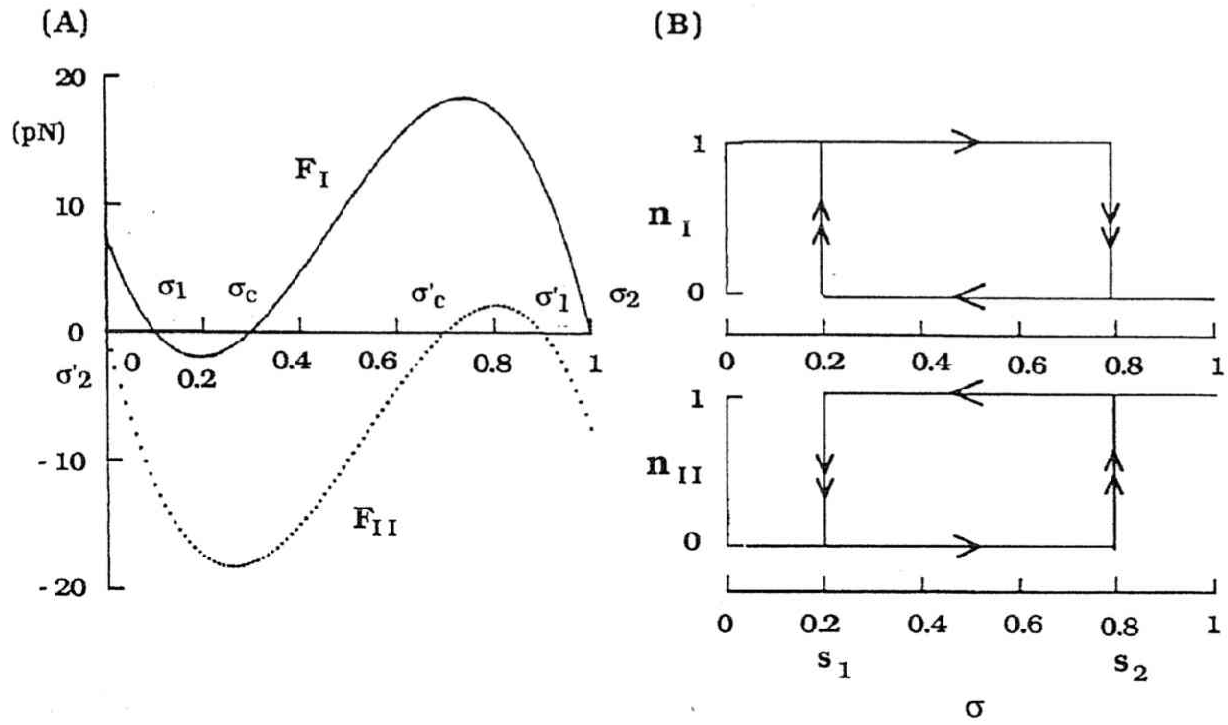
(A)
(B)
20
(pN)
10
0
-10
-20
F_I
F_{II}
σ_1
σ_c
σ'_c
σ'_1
σ_2
σ'_2
0
0.2
0.4
0.6
0.8
1
n_I
n_{II}
s_1
s_2
σ

Fig. 1

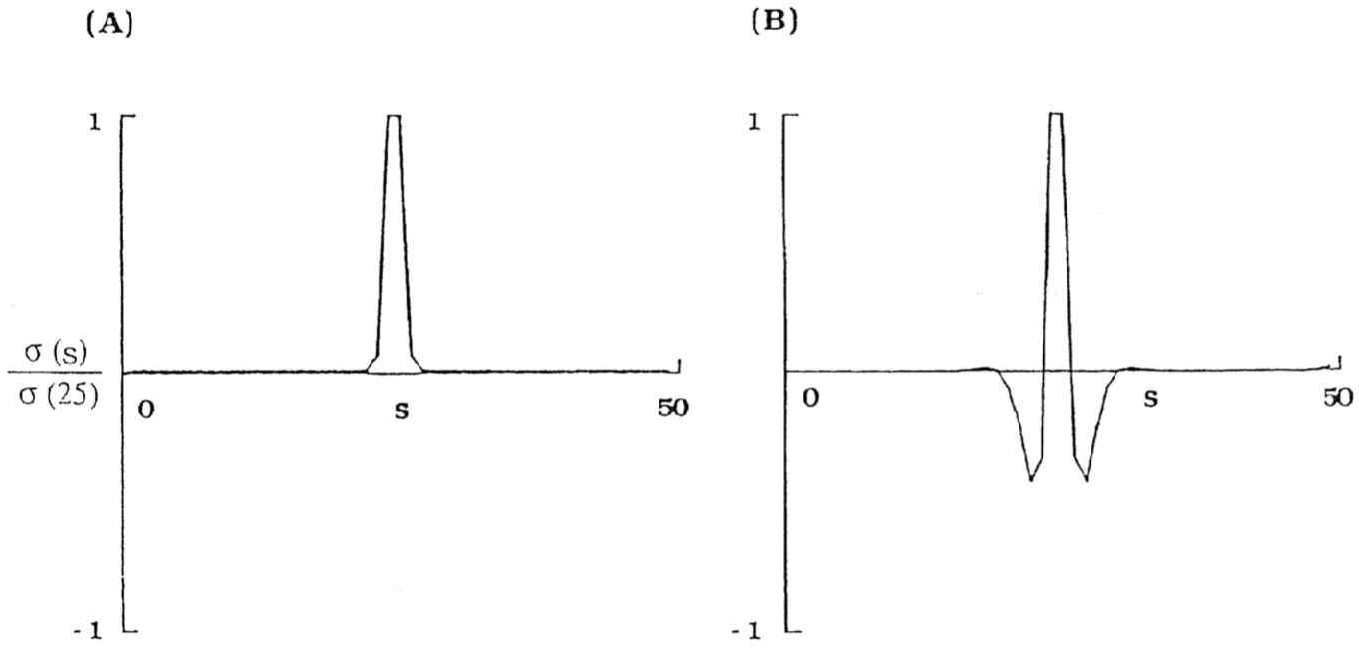

Fig.2

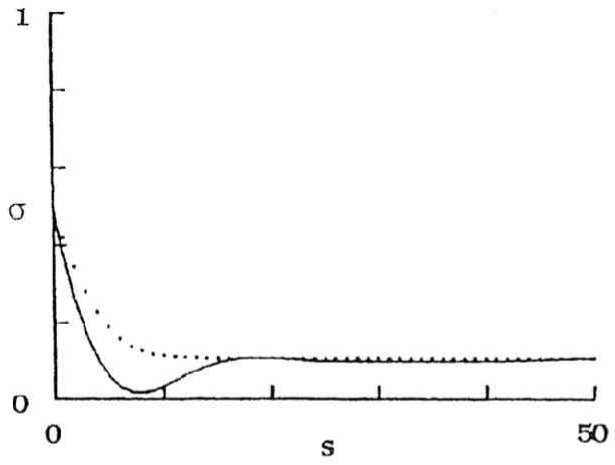

Fig.3

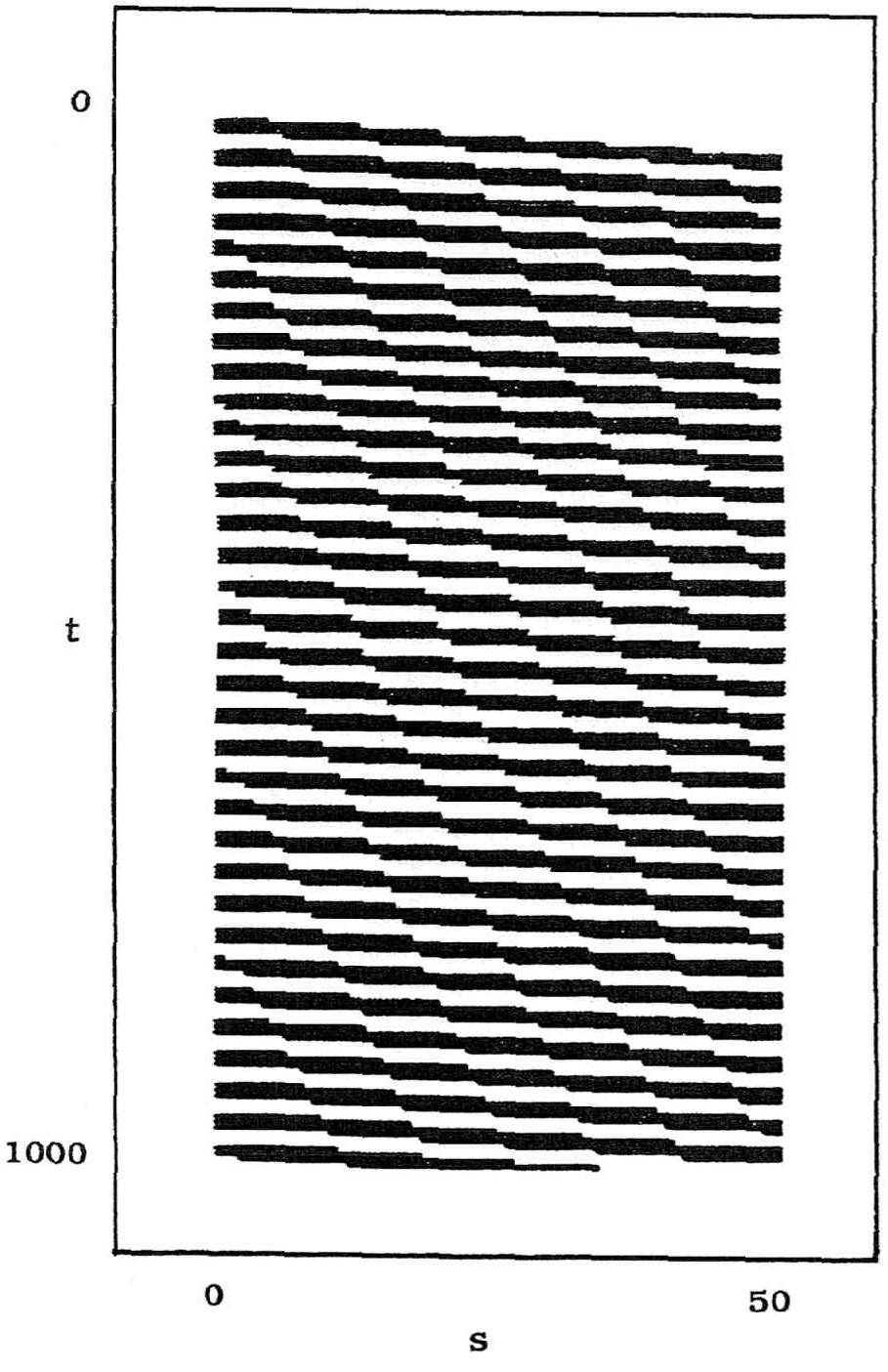
0
t
1000
0
50
s
Excitable region
· At zero external viscosity
· Free end
Oscillatory region

Fig.4

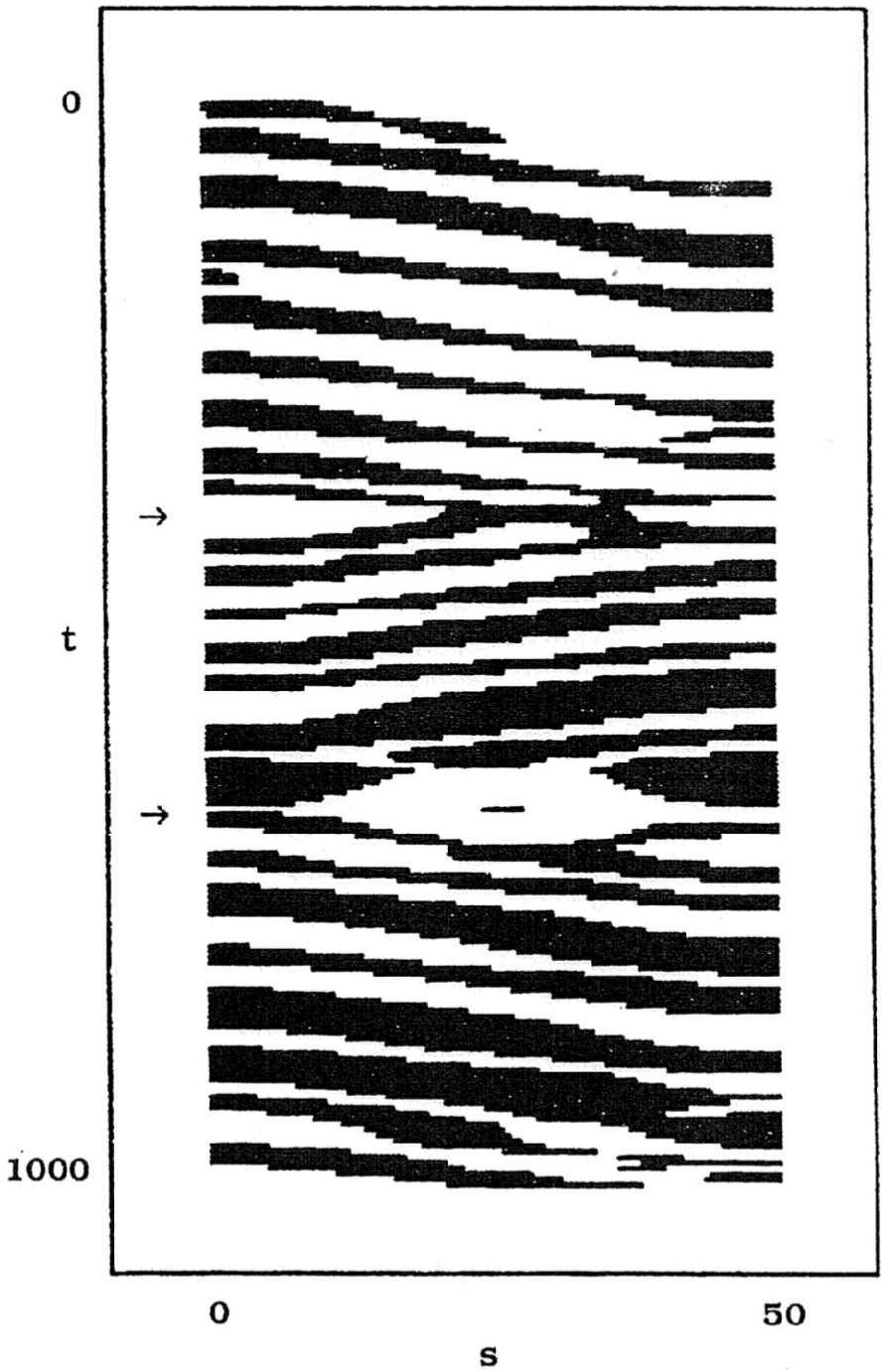
0
t
1000
0
50
s

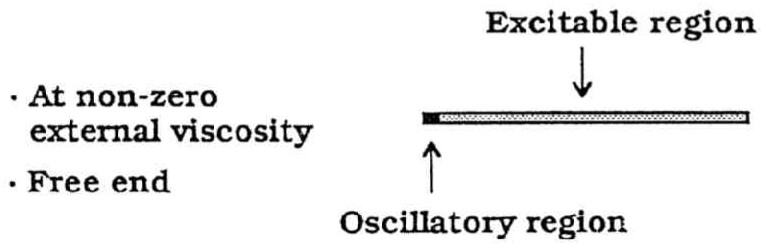
Excitable region
· At non-zero external viscosity
· Free end
Oscillatory region

Fig.5

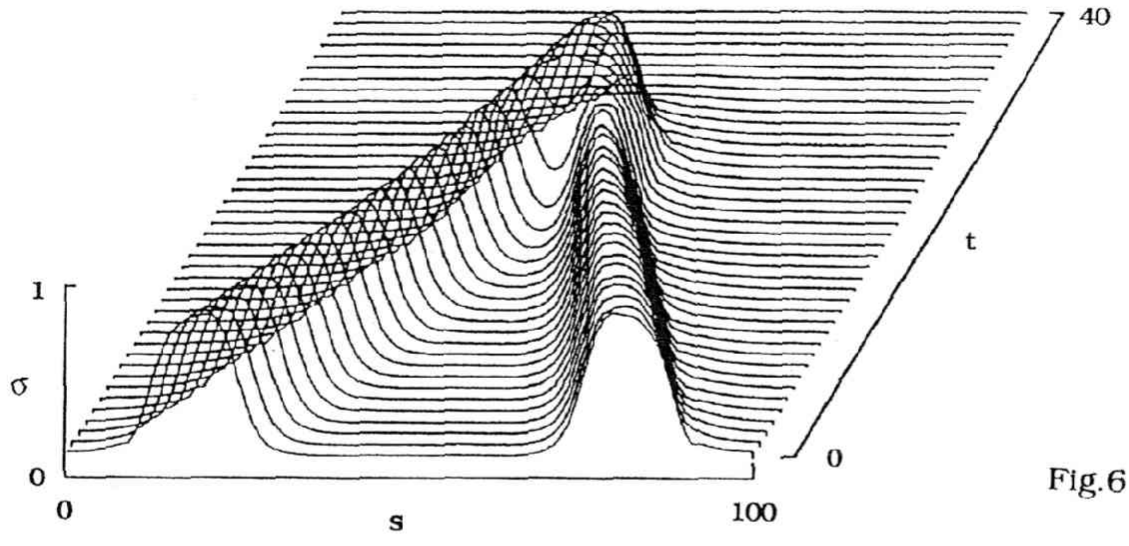

Fig.6

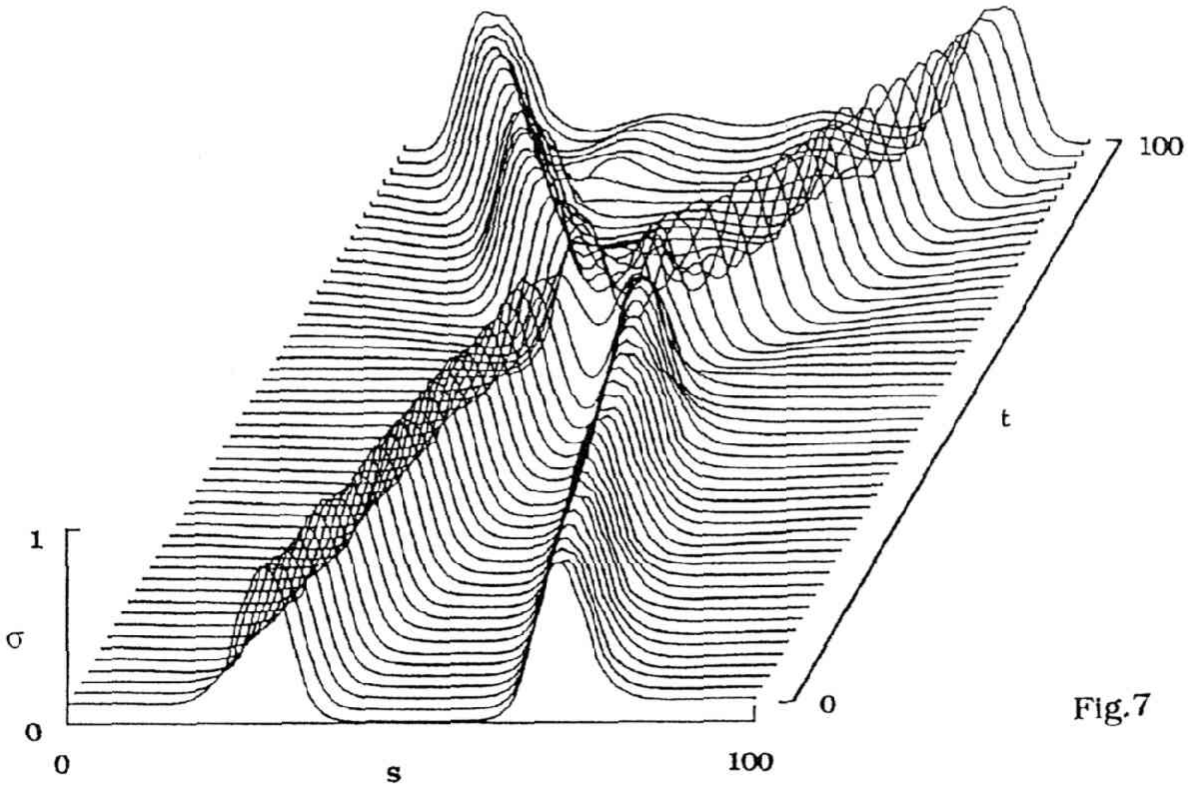

Fig.7

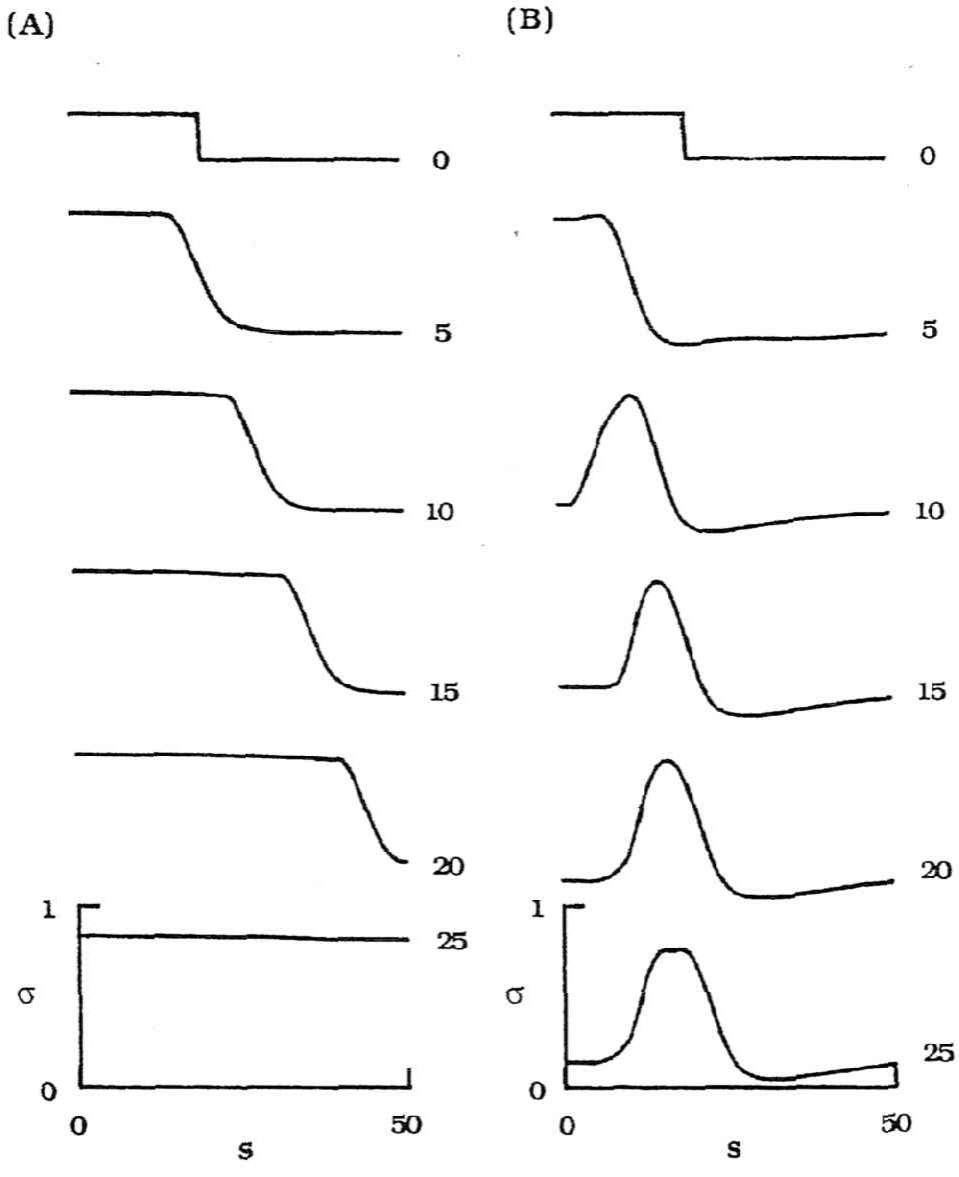

Fig.8

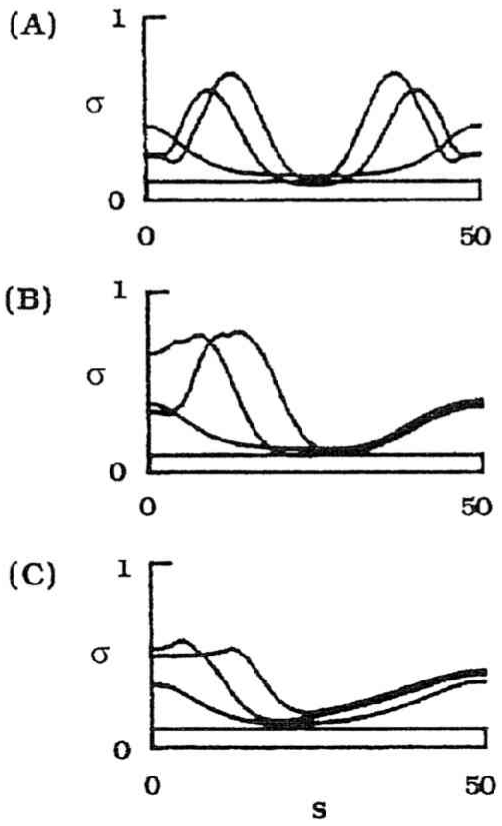

Fig.9